Title
Real-Time Nanomicroscopy via Three-Dimensional Single-Particle Tracking

Journal
ChemPhysChem, 10(14)

ISSN
1439-4235

Authors
Katayama, Yoshihiko
Burkacky, Ondrej
Meyer, Martin
et al.

Publication Date
2009-10-05

DOI
10.1002/cphc.200900436

Published in final edited form as:
Chemphyschem. 2009 October 5; 10(14): 2458–2464. doi:10.1002/cphc.200900436.

Real-time Nanomicroscopy via Three-Dimensional Single-Particle Tracking

Yoshihiko Katayama[1], **Ondrej Burkacky**[1], **Martin Meyer**[2], **Christoph Bräuchle**[1,3], **Enrico Gratton**[4], and **Don C. Lamb**[1,3,5]

[1]Department for Chemistry and Biochemistry and Center for Nanoscience (CeNS), Ludwig-Maximilians-Universität München, Butenandtstrasse 11, 81377 Munich, Germany

[2]Pharmaceutical Biology-Biotechnology, Department of Pharmacy, Ludwig-Maximilians-Universität München, Butenandtstrasse 5–13, Building D, 81377 Munich, Germany

[3]Munich Center for Integrated Protein Science (CiPSM), Ludwig-Maximilians-Universität München, Butenandtstrasse 11, 81377 Munich, Germany

[4]Laboratory of Fluorescence Dynamics, Biomedical Engineering Department, University of California, Irvine, Irvine, CA 92697, USA

[5]Department of Physics, University of Illinois at Urbana-Champaign, Urbana, IL 61801,USA

Abstract

We developed a new method for real-time, three-dimensional tracking of fluorescent particles. The instrument is based on a laser-scanning confocal microscope where the focus of the laser beam is scanned or orbited around the particle. Two confocal pinholes are used to simultaneously monitor regions immediately above and below the particle and a feedback loop is used to keep the orbit centered on the particle. For moderate count rates, this system can track particles with 15 nm spatial resolution in the lateral dimensions and 50 nm in the axial dimension at a temporal resolution of 32 ms. To investigate the interaction of the tracked particles with cellular components, we have combined our orbital tracking microscope with a dual-color, wide-field setup. Dual-color fluorescence wide-field images are recorded simultaneously in the same image plane as the particle being tracked. The functionality of the system was demonstrated by tracking fluorescent-labeled artificial viruses in tubulin-eGFP expressing HUH7 cells. The resulting trajectories can be used to investigate the microtubule network with super resolution.

Keywords

Single Particle Tracking; Scanning FCS; Artificial Viruses

INTRODUCTION

With the development of advanced ultrasensitive fluorescence detection methods, it is possible to perform experiments on single biomolecules and particles. In single molecule experiments, molecules or complexes are typically either immobilized on a surface or snap-shots of individual molecules are collected as they diffuse through the diffraction-limited observation volume of a confocal microscope. A third variation, single particle tracking, allows measurements on individual particles over time scales longer than a few

Corresponding author: Don C. Lamb, don.lamb@cup.uni-muenchen.de, phone: +49-(89)-2180-77564, fax: +49-(89)-2180-77560.

milliseconds. Particularly in the cellular environment, a myriad of information can be gained by following individual biomolecules as they perform their function. Single particle tracking has been used to investigate the movement of lipids in the plasma membrane [1–3], follow individual viruses along their infection pathway [4–6] or study the motion of individual complexes within living cells (e.g. [7,8]).

There has been a large increase during the last years in the development of 2-dimensional and 3-dimensional single-particle tracking methods. In general, two approaches are followed for single-particle tracking: either tracking is performed *ex post facto* from data collected with a camera via post-processing or the tracking is performed in real-time using a feedback approach. The former approach has the advantage that multiple particles can be tracked simultaneously whereas the latter approach is typically faster and more flexible. An elegant variation of the second approach was developed by Cohen and Moerner who used a feedback loop to cancel Brownian motion by electrokinetic forces induced by varying the voltage on electrodes near the particle and thereby trapping the particle [9]. However, this approach is not currently applicable to measurements in living cells.

Two similar methods for 3-D particle tracking using feedback have been realized: tetrahedral tracking by Berg [10] and Werner [11] and orbital tracking by Gratton [12,13]. In the groups of Berg and Werner, four detectors measure different volumes arranged in a tetrahedral geometry about the focus of a confocal microscope and are used to detect motion of a particle away from the focus. The sample stage is then moved to place the tracked particle back into the center of the confocal volume. In orbital tracking, the laser is orbited around the tracked particle. Detection of the *z*-position is performed in two planes, one above and a second below the tracked particle. A feedback algorithm is used to keep the orbit centered on the particle being tracked.

One of the major criticisms of the orbital tracking method is that one is blind to the local environment. Here, we present a modified version of 3-D orbital tracking where wide-field images can be simultaneously collected. Hence, we are able to probe the local environment of the tracked particle while maintaining the advantages of the feedback tracking method. The trajectories determined from tracking individual particles can be used to provide a nanoscopic view of the particles behavior within the context of the living cells. From the trajectories of single particles, the maximum amount of information available regarding the motional behavior of the tracked particle can be gained including the diffusion coefficient, instantaneous and average transport velocities, or corralled radius [14–19]. As the motion within cells is anisotropic, 2D tracking can lead to artifacts and misleading results. With the full, 3D information, the anisotropies can be investigated in detail. In addition, simultaneous wide-field imaging allows visualization of the cellular environment about the individual particles and the interaction of the tracked particles with different cellular components.

MATERIALS AND METHODS

Experimental Setup

A schematic of the experimental setup is shown in Fig. 1a. The custom-built microscope system was constructed around a Zeiss Axiovert 200 inverted microscope base. A Nikon water immersion objective (NA 1.20 63×) or a Zeiss air objective (NA 0.95 60×) were used for the measurements. The objectives were mounted on a piezo objective positioner (MIPOS 100PL CAP, piezosystem Jena). For calibration and test measurements, beads where immobilized on coverslips and mounted on an *x*-*y*-*z* piezo stage (P-517.3CL, Physik Instrumente) which was precisely controlled with two National Instruments Cards (PCI-6036E, PCI-6733, and two BNC-2090). The hardware and data collection for the wide-field and laser-scanning confocal setups were controlled with separate computers. The

orbital tracking was controlled with SimFCS (Globals Software), the piezo stage was controlled with Labview (National Instruments) and the camera was controlled with Andor IQ software (v 1.7). Further details are given in the Supplementary Information.

Cells

Experiments were conducted on HUH7 human hepatome cells where the microtubules were tagged with eGFP. Two days before the measurement, the cells were placed in B27 medium to reduce autofluorescence. For microscopy, the cells were grown in a NUNC chamber and kept 1–2 days in an incubator (37°C and 5 % CO_2 atmosphere) before the experiment. Immediately before the measurements, the medium was exchanged with CO_2 independent medium and mounted onto a microscope heat chamber (TempControl 37-2 digital). We did not use an objective heater as evaporation of the water immersion fluid negatively influenced our experiments.

Polyplexes

DNA plasmids were double-labeled with Cy3 and Cy5 (Label IT Kits, MIRUS) and DNA/polyethylenimine polyplexes were prepared as previously described[20]. The PEIPEG polymers were modified with epidermal growth factor to enhance the uptake efficiency and rate. The polyplexes were stored in aliquots at −80°C until shortly before the measurements, at which time they were first warmed in a heat bath at 36°C and then added to cell culture medium at 37°C. Experiments were started immediately after addition of the artificial viruses and were performed for 3 to 4 hours. The median particle size determined from similar preparations using dynamic light scattering was 266 ± 22 nm.

RESULTS and DISCUSSION

Orbital tracking

Orbital tracking is an extension of scanning FCS [21–23], which was applied to tracking in two-dimensions by Enderlein [24] and in three-dimensions by Gratton [12,13,25]. In orbital tracking, the laser beam is circularly scanned around a particle with a radius approximately equal to the half-width at half-maximum of the point spread function (PSF). When the particle is at the center of the orbit, the measured fluorescence intensity is constant during the orbit (Fig. 1b). However, any movement of the particle from the center of the orbit leads to a modulation of the fluorescence signal. From the phase and amplitude of the oscillations in fluorescence intensity (Supplementary Information and [25]), the direction and radial distance the particle moved from the center of the orbit is determined. To calculate the position of the particle in real time, a fast Fourier transform of the orbit is calculated and the first harmonic determined. A calibration file is used to convert the modulation into a distance. The offsets of the signals used to control the position of the mirror are adjusted to reposition the center of the orbit at the newly determined location of the tracked particle. Depending on the speed of the scanner and the strength of the signal, orbits can be performed on the submillisecond time scale. For the piezo mirror used in our apparatus (a schematic diagram of the setup is shown in Fig 1a), each orbit required 16ms and 2 orbits were averaged together before performing the feedback step. Hence, the time resolution of our system is 32 ms. To achieve this speed with the piezo mirror, the characteristic time response of the piezo had to be calibrated and compensated for (see Supplementary Information). In post analysis, the time resolution can be increased to that of the orbital frequency by evaluating the raw data from the individual orbits.

Tracking in the z-dimension

The above method allows tracking of particles in two-dimensions in real time. Conceptually, one can imagine a similar approach for the third-dimension but it is typically sufficient to monitor two planes, one immediately above the particle and the other immediately below the particle. In the SPT method published previously by Levi *et al.* [13], *z*-tracking was achieved by oscillating the objective between two planes about the focal region with a separation of ~ 1μm. Here, we measure two image planes simultaneously by splitting the fluorescence signal into two separate confocal channels and shifting the axial position of the confocal pinhole in each channel to correspond to image planes slightly above or below the focus plane of the excitation laser. Three-dimensional tracking using two image planes has been applied previously to wide-field microscopy[26–28]. The *x* and *y* positions are determined as described above from the sum of the two detection channels and the *z*-position of the particle is determined from the difference of the two detector channels. Using a piezo-driven objective holder, the focus of the objective is moved to keep the tracked particle centered between the two observation volumes. In the orbital tracking method developed earlier, it was advisable to use air objectives (with an NA < 1) to avoid mechanical coupling of the oscillating objective to the sample. Here, water immersion objectives can be used, which collect more photons due to the higher NA. The fact that the *z*-position of the objective follows that of the tracked particle without an additional oscillation of ±500 nm also allows the simultaneous collection of sharp wide-field images in the focal plane of the tracked particle. The wide-field image will always be from the image plane of the tracked particle, enabling detailed investigations of the interaction of the tracked particle with the cellular environment.

Simultaneous wide-field imaging

A dichroic mirror underneath the objective separates the wide-field detection path from the 3D-SPT microscope. The wide-field detection is divided spectrally into two channels and imaged on different regions of an EMCCD camera. The wide-field channels can be used to image different cellular components with eGFP and/or mRFP and thereby visualize the interaction of the tracked particles with these components. Alternatively, the tracked particle can be double-labeled so that it is in addition directly visible in the wide-field image. In either case, three spectrally separated channels can be investigated simultaneously (our current configuration uses 488 nm, 561 nm, and 633 nm excitation). Due to the real-time feedback in *z*, the focal plane of the tracked particle is always visualized in the wide-field channel. This is demonstrated in Fig. 2 and Supplementary Movie 1. A 170nm multi-color fluorescent bea d (Kisker FP-0257-2, Spherotech, emission maxima at 490 nm, 560 nm and 620 nm) was immobilized on a cover slip and mounted on a three-axis piezo stage. A trajectory mimicking the movement of an actual particle was feed into the piezo stage. The experiment was performed twice, once with wide-field collection in a single *z*-plane without the orbital tracking and a second time with simultaneous orbital tracking. The three-dimensional trajectory along with different images taken during the trajectory with and without orbital tracking are shown in Fig. 2a–c. As the particle diffuses in *z*, it is lost with two-dimensional tracking but remains in focus in the wide-field detection channel during the entire measurement when the particle is being followed with orbital tracking. The given trajectory also demonstrates the advantage of three-dimensional tracking. If motion were purely Brownian, the main advantage of 3-D tracking would be the ability of the system to keep the particle in focus and track the particle over longer times, but the resulting information from analysis of the trajectories would be identical. However, in living cells, motion is often anisotropic and the results from a 2-D analysis inaccurate. For example, a mean-squared-displacement (msd) analysis using a window of 50 data points was performed at each position along the trajectory from either the *x–y* projection (shown in blue in Fig. 2a)

or the full 3D trajectory (Fig. 2d,e). The results are very different demonstrating the advantage of having 3D information.

One of the major criticisms of the 3-D orbital tracking method is the difficulty in knowing whether the tracked particle is always the same particle or whether the focus of the tracking has jumped to another particle during the measurement. Although it may be possible to distinguish when a second particle enters the vicinity of the tracked particle by analyzing the higher harmonics of the fluorescent signal during an orbit, this capability has not yet been demonstrated. By utilizing double-labeled particles, we observe the particles in the wide-field image and we can directly visualize events when the orbital tracking jumps to a second particle (Supplementary Movie 2).

Characterization of the microscope

Tracking Accuracy—To test the stability and accuracy of the system, fluorescence beads were immobilized on a coverslip and tracked over 25 minutes. A fraction of the trajectory of one immobilized particle is shown in Fig. 3a along with the standard deviation of the particle location. Particles with an average fluorescent intensity in the range of 10 – 40 kHz in the two detection channels could be localized with an accuracy of $\sigma_{x,y}$ = ~15 nm and σ_z = ~20 nm. Although absolute accuracies are helpful as a point of reference, they are soft numbers that depend on the signal-to-noise ratio, temporal resolution and motional behavior of the particle. A particle moving at 5 μm/s will transverse 160 nm during the 32 ms needed to calculate the position of the particle and the accuracy of the position determination will be significantly worse than for the stationary case. To test the dynamical response of our system, immobilized multifluorescent beads mounted on a piezo stage were oscillated sinusoidally at different frequencies in either the *x*, *y* or *z* direction (Fig. 3b left panel). To eliminate synchronization difficulties between the particle trajectory controlled with a piezo-stage and the tracking routine of our 3D SPT microscope, we fit the resulting trajectory to a sin function (Fig. 3b middle panel) and compared the amplitude of the fit to the amplitude of the particle motion and analyzed the deviation of the measured data from the fit (Fig. 3b right panel). A plot of the input amplitude, recovered amplitude and standard deviation between the fit and the data are plotted as a function of frequency for *x* and *z* in Fig. 3c and 3d respectively. Up to a frequency of 0.7 Hz at an amplitude of 1.3 μm, corresponding to a maximum velocity of 5.7 μm/s, the uncertainty (one standard deviation) remains below 20 nm in *x* and *y* and around 60 nm in *z*. Above this frequency, there is an increase in the uncertainty of the tracking algorithm and the amplitude of motion is no longer correctly reproduced. For transport processes and the diffusion of protein complexes in live cells, this resolution is more than sufficient. By adjusting the scan radius, pinhole separation and calibration curve used to calculate the position of the particle, our tracking system can be tuned for highest accuracy, fastest response, or an optimal compromise between the two.

The lateral position of a dual-labeled particle can be determined in wide-field as well as with orbital tracking. For the trajectory shown in Fig. 2, the accuracy from a 2D Gaussian fit, estimated from the covariance matrix of the fitting algorithm, is given below the respective images (Fig 2b,c) at different positions along the trajectory. When tracking is turned on, the lateral accuracy remains at around 3 nm while the uncertainty of the purely 2D tracking movie dramatically increases when the particle is out of focus and the particle is eventually lost. The spatio-temporal accuracy of wide-field and the orbital tracking are similar in these measurements as the temporal accuracy of the wide-field images are a factor of 6.25 slower and the spatial accuracy is roughly a factor 5 higher than that of the orbital tracking. With the orbital tracking and simultaneous wide-field imaging, we can utilize either method to determine the lateral position of the particle. Under circumstances where the dynamics are

slow and the tracked particle has a stronger signal in the wide-field channel, the lateral position of the particle can be determined with higher accuracy from the wide-field data.

Tracking of artificial viruses in HUH7 cells

The system was tested by tracking the transport of artificial viruses in living cells. Artificial viruses, in this case DNA polyplexes, are used as vectors in gene therapy [29]. Detailed investigations of particle uptake and transport have shown that these particle initially interact with the actin cytoskeleton and are later transported along microtubules [14,30]. Here, we have investigated the transport of artificial viruses along the microtubules. Egfp-labeled tubulin of the human hepatoma cell line HUH7 were infected with artificial viruses where the plasmid had been fluorescently labeled with Cy3 and Cy5. Individual viruses could be tracked for several minutes. Although photobleaching was observable during the measurement, it did not interfere with the tracking. Fig. 4a shows the 3D trajectory of an artificial virus along a microtubule. Wide-field images from two planes separated by 500 nm are shown with the eGFP-tubulin displayed in green and the artificial viruses in red. The correlation between the trajectory of the particle and the fluorescently marked microtubules verifies that the particles are being transported along microtubules at this stage of infection. During tracking, the artificial virus stalls at a junction between microtubules and moves slowly in a direction lateral to its previous motion before being transported along a different microtubule (Fig 4b). With the information about the local environment of the cell given from the wide-field images, it is easy to see that the slow lateral shift of the virus is due to rearrangement of the microtubule network (highlighted with the white arrow). Such coordinated motion is only detectable with simultaneous wide-field imaging. The average transport velocity of 250 nm/s for the single artificial virus was determined from a msd analysis of the trajectory (Fig 4c).

Knowing that the particles are transported along microtubules, the super-resolution of particle tracking can be used to map out the 3D structure of the microtubules as a function of time. Such detailed, time-dependent information in the axial dimension is not easily obtainable in live-cells with current wide-field or deconvolution methods.

CONCLUSIONS

We have developed a novel single-particle tracking microscope with significant advantages over other 3D tracking methods. The setup combines the advantages of confocal orbital tracking and wide-field imaging. Particles are tracked in real time. Therefore, it is not necessary to preselect a region of interest before the experiment begins and the trajectory is available immediately without post processing. Many of the currently used 3D tracking approaches use two image planes (e.g.[26–28,30]). However, without additional feedback, these approaches are limited to movement in axial dimension of 1–2 μm. Another approach, proposed by Speidel [31], uses the diffraction pattern of the tracked particle to determine its axial position. Here again, the depth over which axial displacements can be determined are limited. By coupling our two-focal plane approach to a feedback loop, the lateral tracking is limited only by the displacement of the piezo-objective holder (100 μm), which is significantly larger than the thickness of most cells.

The two major criticisms of orbital tracking are: 1) only one particle can be tracked at a time whereas wide-field methods can track several particles *ex post facto* and 2) there is no information on what is happening in the vicinity of the particle. When the dynamics of interest is slow enough, multiplexing can be performed and several molecules tracked simultaneously as shown in Levi *et al.* [12]. Visualization of the surroundings can be performed by collecting simultaneous wide-field images. The wide-field microscope can be

used to measure different structures within a cell and/or can be used to visualize the particle being tracked.

Merging wide-field imaging and single-particle real-time tracking leads to a system with powerful capabilities. On the one hand, the wide-field can be used to visualize the interaction of the tracked particles with each other or with cellular organelles. On the other hand, single particle tracking can be used to gain super-resolution information about structures observed in the wide-field image.

Supplementary Material

Refer to Web version on PubMed Central for supplementary material.

Acknowledgments

We wish to thank the laboratory of Prof. E. Wagner for help with the preparation of the polyplexes and Christian Hellriegel and all members of AK Bräuchle for fruitful discussions. We also kindly acknowledge the expert assistance of Monika Franke with the cell culture and Veronika Zinth and Tobias Bluemke for assistance in developing and testing the microscope system. We gratefully acknowledge the financial support of the Deutsche Forschungsgemeinschaft (DFG, SFB646, SFB749 and SPP1175 to C.B. and D.C.L.), the Nanosystems Initiative Munich (NIM) and the LMU-Innovativ BioImaging Network Munich (BIN) to C.B. and D.C.L. and the Bavaria-California Technology Center (BaCaTeC) to E.G. and D.C.L. E.G. also acknowledges support from NIH-P41-RR003155.

References

1. Fujiwara T, Ritchie K, Murakoshi H, Jacobson K, Kusumi A. J Cell Biol 2002;157:1071–1081. [PubMed: 12058021]
2. Schmidt T, Schutz GJ, Baumgartner W, Gruber HJ, Schindler H. Journal of Physical Chemistry 1995;99:17662–17668.
3. Schutz GJ, Kada G, Pastushenko VP, Schindler H. Embo Journal 2000;19:892–901. [PubMed: 10698931]
4. Brandenburg B, Zhuang X. Nat Rev Micro 2007;5:197–208.
5. Marsh M, Helenius A. Cell 2006;124:729–740. [PubMed: 16497584]
6. Seisenberger G, Ried MU, Endress T, Buning H, Hallek M, Brauchle C. Science 2001;294:1929–1932. [PubMed: 11729319]
7. Kubitscheck U, Kuckmann O, Kues T, Peters R. Biophysical Journal 2000;78:2170–2179. [PubMed: 10733995]
8. Lange S, Katayama Y, Schmid M, Burkacky O, Brauchle C, Lamb DC, Jansen RP. Traffic 2008;9:1256–1267. [PubMed: 18485054]
9. Cohen AE, Moerner WE. Proc Natl Acad Sci U S A 2006;103:4362–4365. [PubMed: 16537418]
10. Berg HC. Review of Scientific Instruments 1971;42:868–871. [PubMed: 4940742]
11. Lessard GA, Goodwin PM, Werner JH. Applied Physics Letters 2007;91:224106.
12. Levi V, Ruan Q, Gratton E. Biophys. J 2005;88:2919–2928. [PubMed: 15653748]
13. Levi V, Ruan Q, Kis-Petikova K, Gratton E. Biochemical Society Transactions 2003;31:997–1000. [PubMed: 14505467]
14. de Bruin KD, Ruthardt N, Gersdorff KV, Bausinger R, Wagner E, Ogris M, Brauchle C. Molecular Therapy 2007;15:1297–1305. [PubMed: 17457321]
15. Rust MJ, Lakadamyali M, Zhang F, Zhuang X. Nat Struct Mol Biol 2004;11:567–573. [PubMed: 15122347]
16. Saxton MJ. Biophys J 1993;64:1766–1780. [PubMed: 8369407]
17. Saxton MJ. Biophys J 1994;67:2110–2119. [PubMed: 7858148]
18. Saxton MJ. Biophys J 1994;66:394–401. [PubMed: 8161693]
19. Saxton MJ. Biophys J 1995;69:389–398. [PubMed: 8527652]

20. von Gersdorff K, Ogris M, Wagner E. Eur J Pharm Biopharm 2005;60:279–285. [PubMed: 15939238]
21. Berland KM, So PT, Chen Y, Mantulin WW, Gratton E. Biophys. J 1996;71:410–420. [PubMed: 8804624]
22. Petersen NO. Biophys. J 1986;49:809–815. [PubMed: 3719067]
23. Petersen NO, Johnson DC, Schlesinger MJ. Biophys. J 1986;49:817–820. [PubMed: 3013328]
24. Enderlein J. Applied Physics B: Lasers and Optics 2000;71:773–777.
25. Kis-Petikova K, Gratton E. Microscopy Research and Technique 2004;63:34–49. [PubMed: 14677132]
26. Prabhat P, Ram S, Ward ES, Ober RJ. IEEE Trans Nanobioscience 2004;3:237–242. [PubMed: 15631134]
27. Prabhat P, Gan Z, Chao J, Ram S, Vaccaro C, Gibbons S, Ober RJ, Ward ES. Proc Natl Acad Sci U S A 2007;104:5889–5894. [PubMed: 17384151]
28. Toprak E, Balci H, Blehm BH, Selvin PR. Nano Lett 2007;7:2043–2045. [PubMed: 17583964]
29. Park TG, Jeong JH, Kim SW. Adv Drug Deliv Rev 2006;58:467–486. [PubMed: 16781003]
30. Bausinger R, Gersdorff Kv, Braeckmans K, Ogris M, Wagner E, Bräuchle C, Zumbusch A. Angewandte Chemie International Edition 2006;45:1568–1572.
31. Speidel M, Jonas A, Florin EL. Opt Lett 2003;28:69–71. [PubMed: 12656488]

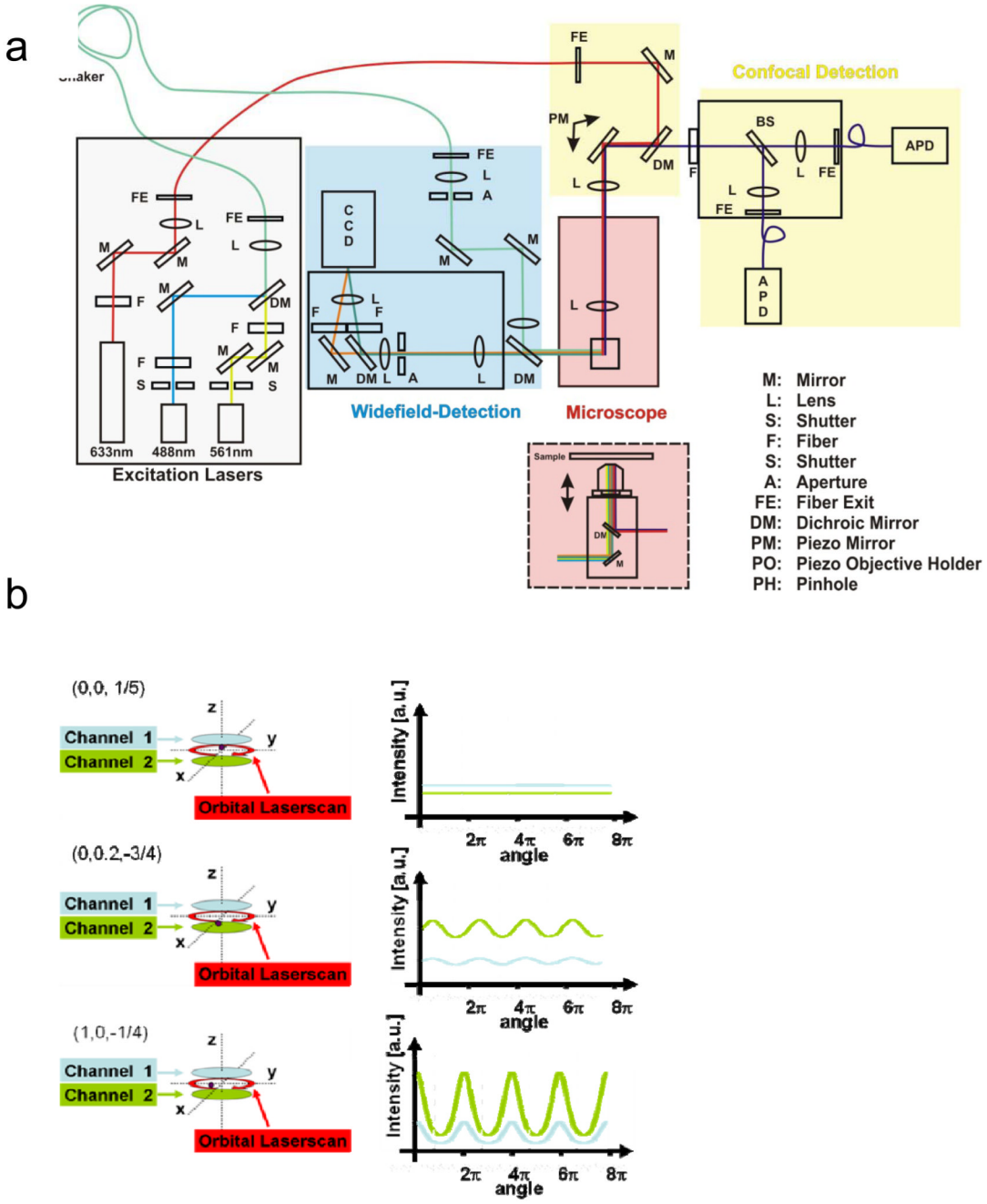

Figure 1. Orbital Tracking

a) A schematic diagram of the experimental setup. The setup consists of four major components, 1) The excitation sources with fiber optic coupling, 2) Wide-field detection, 3) Confocal Detection, and 4) the microscope base where the different fluorescence methods are combined and the sample is mounted. b) The laser beam is scanned about the tracked particle (*left panel*). Depending on the three-dimensional location of the particle, the fluorescence intensity of the particle is modulated during the orbit (*right panel*) as illustrated for 3 possible examples. From the modulation and phase of the fluorescence signal, the *x* and *y* positions of the particle are determined. The *z*-position is determined from the difference in intensity between the two channels.

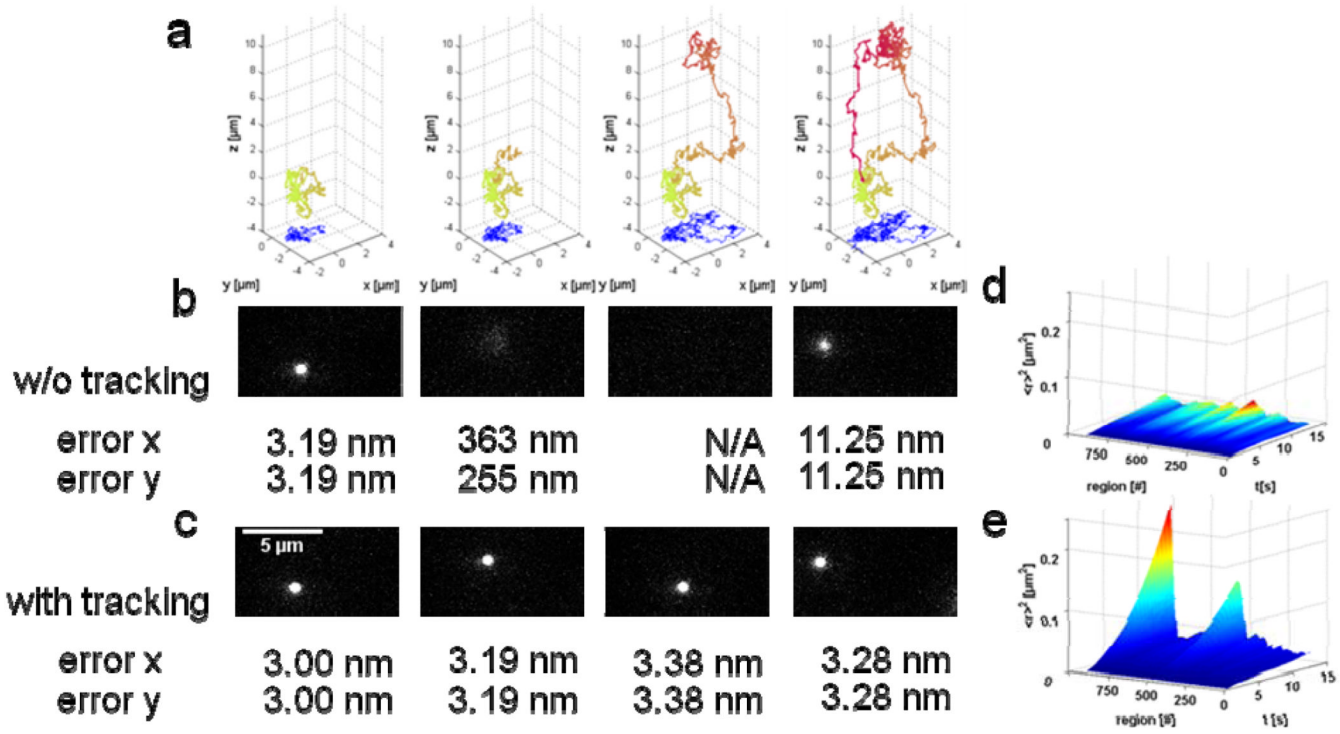

Figure 2. 2D vs 3D Tracking

a) The 3D trajectory of a particle controlled with a 3D piezo table at different positions in time (see Supplemental Movie 2). The 2D projection of the trajectory is shown in blue in the x–y plane. b) The wide-field image of the particle taken in a single *z*-plane without confocal tracking shows the loss and return of the particle in the wide-field image. Accuracies determined from the covariance matrix of a 2-D Gaussian fit of the particle in wide-field is given below. c) The corresponding wide-field images collected with simultaneous tracking and the determined accuracies from the fits to the wide-field images. d–e) The mean-square-displacement for a sliding window of 50 data points along the trajectory incorporating the d) 2D and e) 3D information.

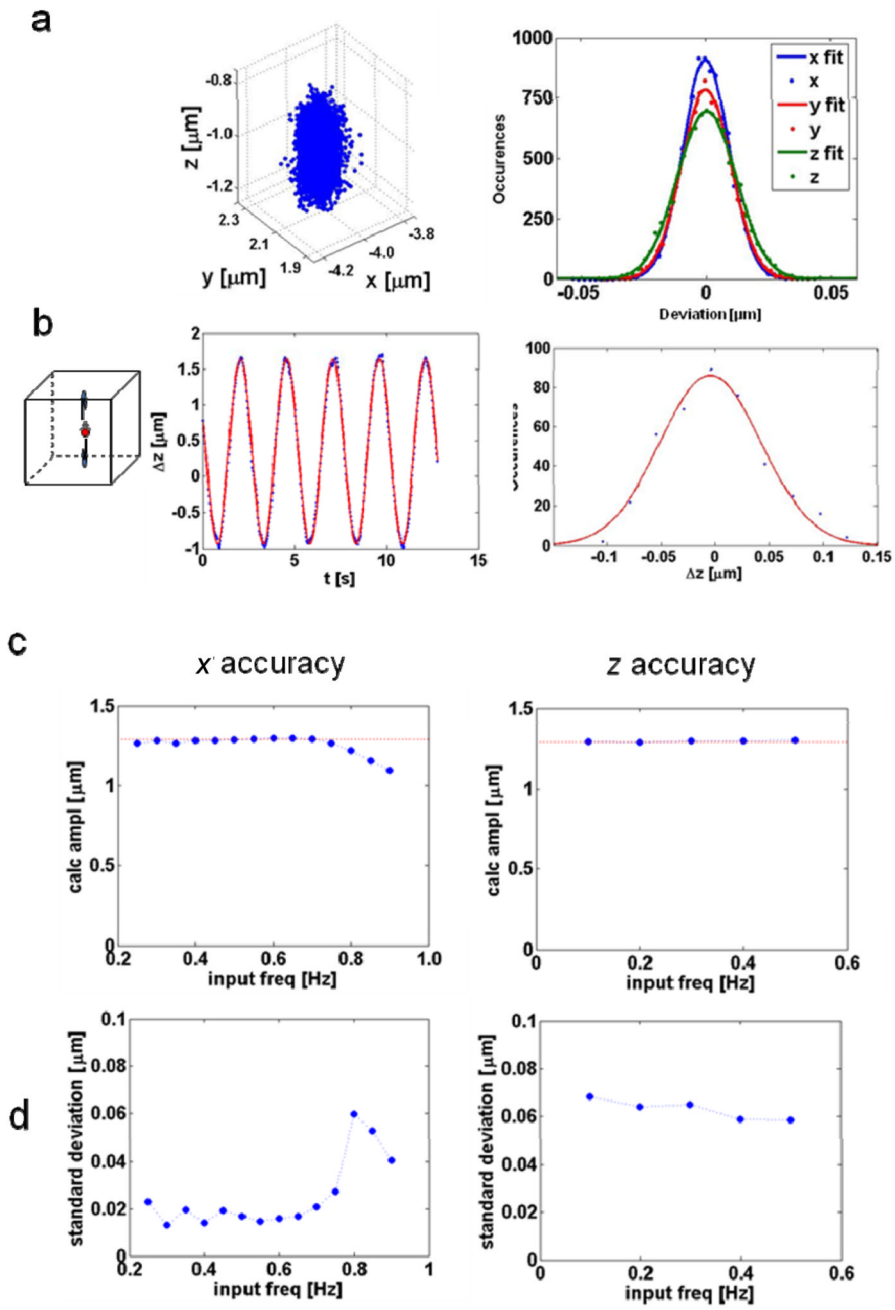

Figure 3. Tracking Accuracy

a) The accuracy of tracking an immobilized particle. *Left panel*, the trajectory of an immobilized particle. *Right panel*, the deviation of trajectory from the average position. The standard deviation of the plots are ~15 nm for the radial dimensions and ~20 nm for the axial dimension. b–d) The accuracy of tracking a moving particle. b) *Left panel*, a schematic showing how a particle was moved sinusoidally in time in one dimension (*z* is shown here). *Middle panel*, The measured position of the particle (data points) and a fit with a sine function (line). *Right panel*, the deviation of the measured position of the particle with the fit. These experiments were performed at various frequencies (between 0.2 and 0.9 Hz) and the amplitude and accuracy determined. c). The input (dotted line) and retrieved amplitude

(data points) of the sine wave used for dynamic testing as a function of frequency for *x* (*left panel*) and *z* (*right panel*). d) The standard deviation of the retrieved data to the fit of a sine wave plotted versus frequency for the measurements shown in panel c.

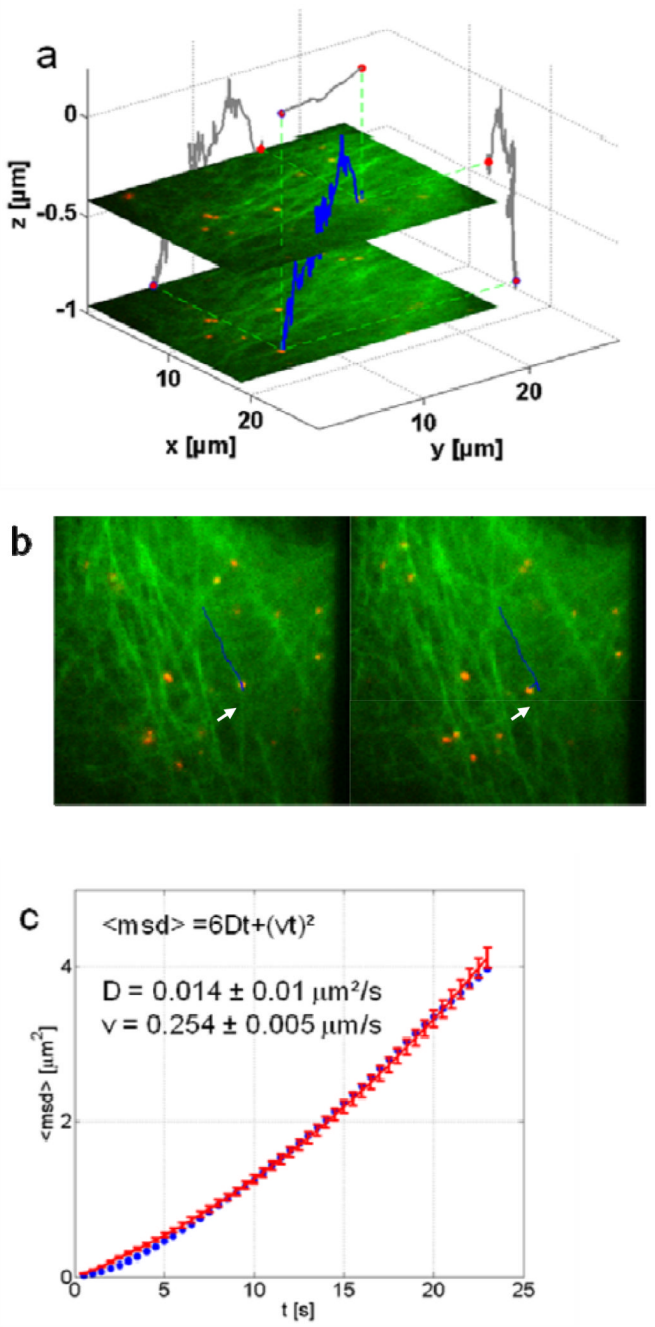

Figure 4. Tracking of Artificial Viruses

a) A 3D trajectory (blue) of an artificial virus (red) in a live HUH7 human hepatome cell transfected with eGFP-tagged tubulin (green) along with two wide-field images taken at different *z*-positions during the measurement. 2D projections of the 3D trajectory are shown in grey on the respective axes. b) Two snapshots from the movie showing (*left*) the virus traveling upwards along a microtubule fiber and (*right*) the virus switching to a different microtubule. The lateral motion observed as the virus switches microtubules is due to motions of the microtubule network (indicated by the white arrows) and not motion of the virus along the microtubule as determined from the wide-field images (see Supplemental Movie 3). c) An msd analysis of the portion of the trajectory shown in blue in panel b (*right*

side). The concave upwards curvature of the msd is characteristic for transport phenomena. The average velocity of transport during this phase of directed motion is ~250 nm/s.